Behavioral/Systems/Cognitive

# Early Skill Learning Is Expressed through Selection and Tuning of Cortically Represented Muscle Synergies

**William J. Kargo and Douglas A. Nitz**
The Neurosciences Institute, San Diego, California 92121

**Skill learning may be based on integrating and adapting movement building blocks organized in the CNS. We examined at what level integration and adaptation occur during early skill learning, the level of individual muscles, muscle synergies or combinations of synergies through time, and whether these operations are expressed through the primary motor cortex (M1). Forelimb muscle and M1 cell activity were recorded over the first day of training on a reach-to-grasp task in rodents. Independent components analysis was used to assess how well muscle activation patterns could be described as time-varying combinations of synergies. In 3 of 11 animals, prereach M1 activity predicted the activation of different combinations of independent components (ICs) to perform the task. With training, animals increasingly adopted postures and prereach patterns of M1 activity that supported activation of the more successful combination. With training, animals also adjusted the activation magnitude (6 of 11 animals) and weights (11 of 11) of specific ICs that constituted the selected combination. Weights represent how IC activation patterns were distributed to forelimb muscles; this distribution pattern was adapted with training. M1 cells (37 of 100) had task-related firing rates that were significantly correlated with IC activation patterns. Changes in M1 firing rates were associated with corresponding changes in either the activation magnitude or weights of the correlated IC. Our data suggest that early skill learning is expressed through selection and tuning of M1 firing rates, which specify time-varying patterns of synergistic muscle contractions in the limb.**

*Key words:* **motor cortex; motor learning; EMG; muscle synergy; movement; kinematics**

## Introduction

Motor skill learning may be based on integrating and adapting movement building blocks organized in the CNS (Mussa-Ivaldi and Bizzi, 2000). Muscle synergies represent one type of building block. Synergies refer to task-dependent muscle groupings controlled by the CNS as a single degree of freedom (Bernstein, 1967). Evidence for such modules is based on findings that subjects scale, phase shift, combine, and reuse muscle synergies to generate various behaviors (Grillner, 1981; Raasch and Zajac, 1999; Tresch et al., 1999; Kargo and Giszter, 2000a). A second type of building block, termed motor program (Morris et al., 1994), refers to the manner in which multiple synergies are activated through time in the absence of significant feedback effects. CNS structures generating motor programs have been termed pattern generators (Grillner, 1981) or internal controllers (Wolpert et al., 2001). Evidence for such modules is based on findings that subjects scale, blend, and switch between discrete, temporally complex motor patterns (Wolpert and Kawato, 1998; Earhart and Stein, 2000; D'Avella et al., 2003).

It is unclear how synergies and motor programs are integrated and adapted at the onset of skill learning and where in the brain such operations are expressed. The primary motor cortex (M1) is an interesting structure with respect to this question because M1 is strongly engaged during motor learning (Pascual-Leone et al., 1994; Kleim et al., 1998; Nudo et al., 1996; Karni et al., 1998; Wise et al., 1998; Li et al., 2001; Muellbacher et al., 2002), encodes muscle activations (McKiernan et al., 2000; Graziano et al., 2002; Holdefer and Miller; 2002; Jackson et al., 2003), and contributes to action selection (Kettner et al., 1996; Carpenter et al., 1999; Laubach et al., 2000). To address the role of M1 in early skill learning, we recorded patterns of forelimb muscle and M1 cell activity over the first day of training on a reach-to-grasp skill in rodents. Learning this skill has been correlated with changes in M1 representations (Kleim et al., 1998), synaptic strengths (Rioult-Pedotti et al., 1998, 2000), and synapse numbers (Kleim et al., 2002).

We hypothesized that early improvements on the reach task occurred at the level of individual muscles, muscle synergies, or motor programs. To test these alternatives, we used independent components analysis to assess how well muscle activation patterns could be described as time-varying combinations of synergies. We determined whether animals increased the probability of activating specific synergy combinations over time. We determined whether the timing or amplitude of synergies comprising specific combinations were adapted. We also determined whether synergy compositions were adjusted with training, which supports individual muscle regulation. Finally, we examined how M1 firing rates were related to changes in muscle, synergy, and motor program activations. Our results provide evidence for parallel mechanisms of early skill learning and for expression of learning through task-related M1 assemblies.

Received May 30, 2003; revised Oct. 6, 2003; accepted Oct. 7, 2003.

This work was supported by the Neurosciences Research Foundation. W.J.K. is the Clayson fellow in Motor Control. We thank M. Kuoppamaki for assistance with surgeries, training, and electrode fabrication, G. Davis, who performed histology, and J. Krichmar and J. McKinstry, who provided useful comments.

Correspondence should be addressed to William J. Kargo at the above address. E-mail: kargo@nsi.edu.

 0270-6474/03/2311255-15$15.00/0

## Materials and Methods

*Animals and presurgical training.* Eleven Sprague Dawley rats weighing 240–360 gm were handled daily 1–3 weeks before surgery. One week before surgery, animals were given a restricted diet (two or three food pellets per night) and trained to run back on a runway to obtain sugar pellets (20 mg; Research Diets, Inc.). One day before surgery, animals were placed in a reach box that had a vertical opening at one end and an outside attached tray (Whishaw and Gorny, 1996). Pellets were positioned on the tray so rats could retrieve pellets with the tongue. Subsequent pellets were placed out of the reach of the tongue to force reaching. After four or five consecutive attempts with the right or left forelimb, rats were categorized as right- or left-handed. Rats displayed clear handedness in this task even at the earliest stages of testing (Hyland and Jordan, 1997).

*Surgery.* Rats were anesthetized intraperitoneally with Nembutal (50 mg/kg, i.p.) and supplemented as needed for the remainder of surgery with Isoflurane. The animal was placed on a heated water pad. The breathing rate and response to a tail pinch were assessed throughout surgery to monitor the anesthesia level. Betadine was applied to skin areas where two or three small incisions were made on the forelimb over target muscles. A single dose of cefazolin (antibiotic, 22 mg/kg, s.c.) was administered. Target muscles were implanted with a pair of EMG wires (single-stranded, Teflon-coated, stainless steel wire; A-M Systems, Inc.), which had a hardened wax ball at one end preceded by a 1–2 mm exposure under the ball. Wires were inserted into the muscle belly and pulled through until the ball came to rest on the belly. EMG wires were braided, tunneled under the skin to a scalp incision, and soldered into pin connectors. Fascia and skin incisions were closed with a suture. Ten to 12 muscles were implanted in each rat. The muscles included, from proximal to distal (primary anatomical functions in parentheses), cervical part of the trapezius (scapular stabilization), cervical part of the pectoralis major (shoulder adduction and flexion), clavicular part of the deltoid (shoulder flexion), teres major (shoulder extension and internal rotation), lateral head of the triceps (elbow extension and shoulder abduction), medial head of the triceps (elbow extension and shoulder extension), long head of the biceps brachii (elbow flexion and supination and shoulder flexion), brachialis (elbow flexion), flexor carpi ulnaris (FCU) and flexor carpi radialis (FCR) (wrist and finger flexion), and extensor carpi ulnaris (ECU) and extensor carpi radialis (ECR) (wrist and finger extension).

The fascia on the skullcap was removed; bleeding vessels were cauterized; and the skullcap was dried with an etchant (3M; purchased through Henry Schein). Bone screws were placed around the skullcap, and a ground screw was placed 2–3 mm rostral and 1–2 mm lateral to bregma. A small window spanning 2–5 mm lateral to bregma and 0–3 mm rostral to bregma was drilled through the skull. Dura covering the exposed motor cortex (M1) was removed. An array of stereotrode microelectrodes (25 $\mu$m Teflon-coated tungsten wires twisted together, gold-plated tips with 5–10 M$\Omega$ resistance) was stereotaxically placed over M1, 2.5 mm lateral and 1.0 mm rostral to bregma. The array was lowered 0.5 mm into M1, and the exposed window was filled with agarose (0.9% in water). The array was then lowered slowly 1.1 mm to layer 5. The array and EMG connectors were secured to the skull bone screws with dental cement.

Correct placement of the array into forelimb M1 was assessed at the end of training. Animals were anesthetized with ketamine (50 mg/kg) and xylazine (10 mg/kg). A stimulus train (300 msec in duration, bipolar pulses, 0.5 msec duration, 20–60 $\mu$A, 200 Hz) was delivered through each wire, and evoked responses were observed. Stimulation through most electrodes evoked forelimb responses and sometimes combined forelimb–vibrissae (or face) responses. After stimulation, animals were deeply anesthetized and perfused with 4% paraformaldehyde. Fixed brain tissue was analyzed for the depth and site of electrode tips. Analysis of brain tissue showed no evidence for obvious cortical damage, including dimpling of superficial layers. Furthermore, mean learning curves were comparable with other published data (Kleim et al., 1998; Bury and Jones, 2002).

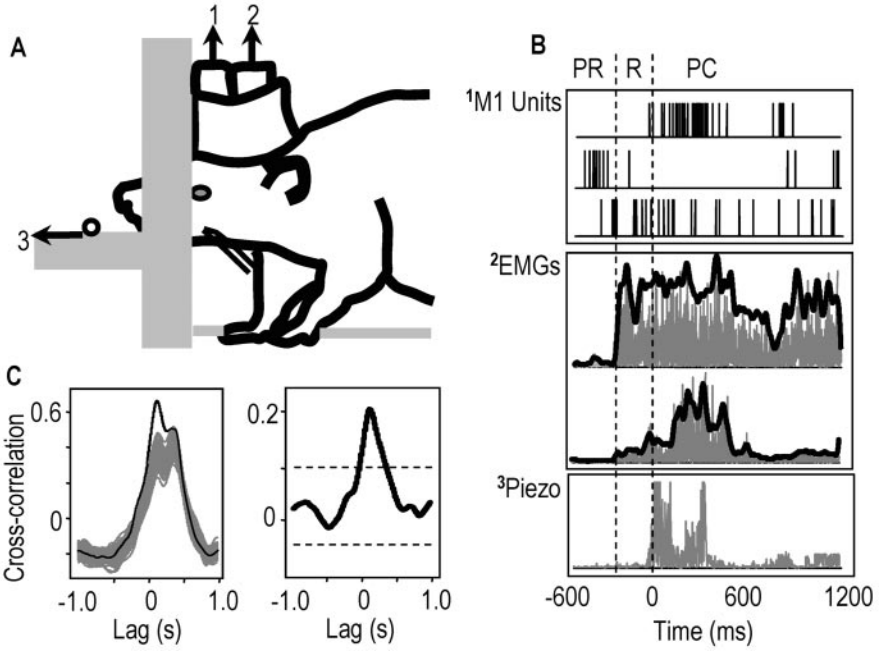


**Figure 1.** *A*, Task setup. Rats reached through an aperture for sugar pellets. Data were recorded from stereotrode arrays in motor cortex (1; M1), forelimb EMG electrodes (2), a piezoelectric strip (3; pellet contact), and a video camera (lateral, top views). *B*, Example data for a reach trial. Top graph, Spikes from three M1 cells; middle graph, rectified EMGs (gray lines) and filtered EMGs (black) from deltoid (top) and biceps (bottom); bottom graph, rectified piezoelectric voltage. PR, Period preceding reach onset (reach onset was the onset of the deltoid EMG burst); R, period between reach onset and pellet contact (contact was the onset of high amplitude piezoelectric activity); PC, postcontact period. *C*, Example of the shift predictor correction of cross-correlations between firing rates of an M1 cell and EMGs. Left graph, Black line, Cross-correlation between time-matched cell activity and EMGs at lags of $\pm$1.0 sec; gray line (75 superimposed lines), cross-correlation between time-shifted cell activity and EMGs (see Materials and Methods). Right graph, Corrected cross-correlation after subtraction of the mean shift predictor (dashed lines, 95% confidence intervals).

*Data acquisition.* Beginning 2 d after surgery, rats were exercised daily on the runway task. EMG and array connectors were secured to the amplifier deck via a tethered wire system. Each tether had a preamplifier array (field-effect transistor; NBLabs, Denison, TX) to increase the signal-to-noise ratio and an array of infrared diodes to track the head position with an infrared camera at 60 Hz. EMG signals were filtered (0.1–3 kHz), and amplifier gains were adjusted on the basis of on-line computer displays to prevent signal saturation. EMG data were digitized at 1–3 kHz and stored on a hard disk using custom-written software (Matt Wilson, Massachusetts Institute of Technology, Cambridge, MA). Signals from individual stereotrode wires were filtered (0.6–6 kHz), and amplitude thresholds for triggering data collection ($\pm$5 msec) were individually set for each wire. An amplitude-crossing event on one wire triggered data collection for the stereotrode pair.

The reach-to-grasp training was initiated 5–7 d after surgery (see setup in Fig. 1*A*). A digital video camera was placed 15 feet away and perpendicular to the long axis of the reach box. A second CCD camera was placed 1 foot above the box and focused on the tray where the sugar pellets were placed. Each camera recorded data at 30 frames or 60 fields/sec. A piezoelectric strip (6 inches long, 1 inch wide, and 0.01 inch thick; Measurement Specialties, Inc.) was placed on the tray. Voltage levels

across the strip were amplified, stored on a hard disk at 1–3 kHz, and synchronized to EMG data. The piezoelectric strip was extremely sensitive to small forces; therefore, it monitored precisely the time at which the animal's hand contacted the tray.

The following procedure was used to synchronize EMG and video data approximately. The first video field in which the hand contacted the tray was estimated and termed field 1. The onset of contact forces was termed contact time 1 (in milliseconds). All video fields were transferred to a hard disk (Sony Digital Video Editor) and were time-matched to EMG data by the following: (field number * contact time 1)/field 1, where field number is the current video field. In the present study, we did not attempt to relate muscle activation to limb kinematics or dynamics in a rigorous manner. This requires precise EMG motion synchronization and high-speed film. The main aim of the present study was to quantify how patterns of muscle activity and M1 activity change during skill learning. Thus, we monitored changes in a few key kinematic parameters (see below) and related these changes to motor pattern changes.

On each day of training, animals were placed into the reach box. A single pellet was placed on the outside tray. Successes and failures were monitored on-line through manual key presses, which marked on EMG records the timing of the event. A successful trial was one in which the rat reached through the aperture, grasped the pellet, and retrieved and brought the pellet to the mouth. Failures were reaches that missed, failed to grasp, or dropped the pellet before reaching the mouth. After each trial, rats were given 30 sec to 1 min before another pellet was placed on the tray. This was to prevent sequential or overlapping reaching movements and to encourage the rat to back away from the opening between attempts. Each rat was given ~100–130 pellets/d (one session/d) for a total of 10 d.

*Data analysis.* EMGs were analyzed off-line using Matlab (MathWorks, Natick MA). Data for each training day (~30–60 min) were parsed to provide 3 sec of EMG data before and after tray contact for each reaching attempt. Parsed EMG records were rectified and filtered with a 40-point tapered boxcar filter (Kargo and Giszter, 2000b).

Four procedures were performed on EMG data: quantification of individual muscle EMGs, measurement of pattern similarity during training, decomposition of EMG patterns into underlying variables using temporal independent components analysis (tICA) and discriminant analysis of successful and failed patterns. Individual EMGs were analyzed for peak amplitude, time of peak amplitude, and burst duration (half-peak onset to half-peak offset) during the period 2.0 sec before and 2.0 sec after tray contact. For muscles with multiple bursts of activity, burst duration was determined for each identifiable burst. To analyze within-day effects, we divided the day 1 training session into three successive blocks with equal numbers of reaching attempts per block (~30–40 attempts per block). Paired *t* tests were used to test for significant differences in EMG parameters between (1) successes and failures, (2) first and last thirds of successes, and (3) first and last thirds of failures on each day.

We calculated motor pattern similarity between the pattern of each trial and the mean successful motor pattern. To calculate pattern similarity, the EMG (rectified and filtered) of each muscle across the training session was normalized to its peak magnitude so that a particular muscle did not dominate the 12-dimensional EMG vector; e.g., EMG magnitudes might differ depending on electrode placement, signal-to-noise quality, and muscle size, and small muscles might have large effects attributable to having large moment arms or actions at the wrist and fingers, which have smaller masses. Thus, at each time point of the reach (in milliseconds), each muscle potentially contributed equally to a 12-dimensional EMG vector. The 12-dimensional vector was then normalized to a unit vector with magnitude of 1.0. This was done at each time point from 2.0 sec before to 2.0 sec after pellet contact. We normalized the EMG vectors because we were interested in whether the balance (or ratio) of muscle activity at a particular time point during the reach changed across the first day of training. The dot product was calculated for time-matched unit vectors (e.g., EMG vector at 50 msec for trial 1 · mean EMG vector at 50 msec, where · refers to the dot product operator). A dot product of 1.0 represents perfect similarity between vectors, and –1.0 represents oppositely pointing, or most dissimilar, vectors. In addition to comparing muscle balance across time, we determined the magnitude of the (un-normalized) EMG vector across time and compared magnitudes between failures and successes and between early- and late-reaching blocks.

EMG patterns for the first day of training were decomposed into a plausible set of underlying synergies using tICA. In its simplest form, the problem of tICA is to separate $N$ statistically independent inputs, which have been mixed linearly in $N$ output channels, without further knowledge about their distributions or dynamics (Makeig et al., 1997). In its application to EMG data, it is assumed that the output of each EMG channel is a time-varying signal mixture $x_i = \{x_i^1, x_i^2, \ldots\}^t$. Each EMG channel receives activation from several underlying (neural) source signals, $s_j$, and each source distributes its signal to multiple muscles. The mixing matrix $A_{ij}$ specifies the relative (linear) contributions of the source signals $\mathbf{s}$ to each channel $x_i$. This linear transformation can be reversed to recover an estimate $\mathbf{u}$ of the source signals $\mathbf{s}$ from the EMG signals $\mathbf{x}$, $\mathbf{s} \approx \mathbf{u} = \mathbf{x}W$, where the separating matrix $W = A^{-1}$ is the inverse of $A$. This separating matrix $W$ maps the set of $N$ mixtures $\mathbf{x}$ to a set of $N$ source signals $\mathbf{s} \approx \mathbf{u}$. To recover an estimate $\mathbf{u} = \mathbf{x}W$ given the assumption that the source signals are mutually independent, ICA iteratively adjusts the separating matrix $W$ to make the estimated source signals $\mathbf{u}$ mutually independent. This is achieved by adjusting $W$ until the entropy of a fixed function, $g$, of signals recovered by $W$ is maximized (where $g$ is assumed to be the cumulative density function of the source signals; Makeig et al., 1997; Stone, 2002). Because maximum entropy signals are independent, it can be shown that this ensures the estimated source signals recovered by $W$ are also independent.

In the present study, ICA was performed using the ICA toolbox for Matlab (Scott Makeig, University of California San Diego, San Diego, CA; Makeig et al., 1997). For purposes of standardizing usage of this toolbox in other EMG studies (in rodents), we used the algorithm as follows. First, we input a matrix $\mathbf{x}$ where the rows were the EMG signals from individual muscles, and the columns were time points (in millisecond intervals). The algorithm zero-means each EMG signal and then computes and applies a sphering matrix $s(m,m)$, where $m$ is the number of EMG channels, to zero-phase whiten the EMG data across time; the EMG data has length, $l$, in milliseconds, e.g., 90 trials × 4.0 sec (wherein each trial is ±2.0 sec relative to pellet contact). The program outputs a matrix $u$ in which the rows are the time courses of activation of the ICA components and a matrix $W$ in which the columns of $W^{-1}$ are the relative projection strengths of the respective components at each EMG electrode pair. The unmixing matrix $W^{-1} = A$ was used to calculate how much of the EMG signal $x(:,l)$ was accounted for by source signal $j$ by $A(:,j) * u(j,l)$.

In repeated trainings, the Matlab random-number generator will cause the ICA toolbox program (runica.m) to deliver the EMG data to the training algorithm in different random orders. This had little effect on the outcome; components with large projections were unchanged, although small components did vary somewhat. However, we were always interested in the first five to seven components (a reduced description of the EMG data), which accounted for the largest (70–85%) percentage of EMG variance and were the same from ICA training session to session. In the 11 rats forming this study, a few (five to seven) underlying source signals, $u$, described ≥80% of the EMG signal, $x$; therefore, tICA performed well at reducing the dimensionality of the 10–12 muscle data set. In the present study, we termed the set of muscles that had $W(j,:) > 0.0$ a synergy (e.g., belonging to synergy $j$). The weights $W(j,:)$ represent the muscle distribution pattern of the underlying source signal.

We performed tICA to address two questions. First, tICA was performed on the entire day's training session to test whether underlying source signals or synergies with constant $w$ are activated differently (e.g., in amplitude or timing) in the first versus the last third of trials. Second, tICA was performed incrementally over $M$ trial segments 1 to $N - 1$ [e.g., trials 1–10, 2–11, . . . $(N - 9)$, to $N$, where $N$ is the number of attempts and $M = N - 9$] to test whether the weight matrices change during training. To assess whether the weights of the most similar synergies changed significantly across trial segments, we computed the Euclidean distance between $w_1(i,:)$ and $w_M(i,:)$ by $[w_1(i,:) - w_M(i,:)] * [w_1(i,:) - w_M(i,:)]'$, where $'$ denotes the transpose. This measure was used in addition to using the dot product because it was very sensitive to changes in the weights vector of an IC, and we were interested in detecting poten-

tially small changes during training, e.g., the range of distance measures between the vector (1.0, 0.5) and the vectors (1.0, 0.6), (1.0, 0.7), and (1.0, 0.8) is 0.3 U, whereas the range of dot product measures is 15 times less, or 0.019 U. We used the dot product measure in addition to verify that, primarily, the balance of weights was changing, and not simply the magnitude (or scaling), because ICs that are returned by the algorithm may be subject to some degree of arbitrary scaling. In addition to reach ICs, we computed the mean Euclidean distance between the weights of the most similar locomotor synergies, which were extracted during lap running before and then after the reach session. We reasoned that locomotor synergies and their corresponding weights should not change over time. Thus, if the Euclidean distance between reach weights fell outside 2 SD of the mean locomotor distance, we considered the reaching weights to change significantly with training (at $p < 0.05$).

Discriminant analysis was used to test how well behavioral success and failure could be predicted from EMG and M1 activity patterns. Discriminant analysis was performed using the Matlab Statistics toolbox. This discriminant algorithm classified the pattern of each trial (EMGs and M1 cells) into either success or failure on the basis of a prespecified training set (composed of 1/10 of the day's reaching attempts, i.e., ~20 reaches). The algorithm fit a multivariate normal density function to each of the specified groups in the training set (success or failure), with a pooled estimate of covariance, and then returned an estimate of the misclassification error rate for the entire set of reaching attempts.

Fuzzy c-means clustering (FCM) was used to assess how well motor patterns clustered into distinct types. We determined the peak activations of ICs on each trial. This set of values (on one trial) formed a 10-dimensional vector in the case in which 10 muscles were recorded and 10 ICs were obtained with ICA. For 100 trials, there were 100 ten-dimensional vectors. These vectors occupied some multidimensional space. We assessed how well FCM could group the vectors into a specific number of different clusters within this space. We used the Fuzzy Logic toolbox in Matlab to perform FCM. FCM assigned each vector a membership grade to a cluster and iteratively updated the cluster centers and membership grades for each vector. The iteration was based on minimizing an objective function that represented the distance from any given vector to a cluster center weighted by the membership grade of that vector.

To determine goodness of clustering, we compared our data with simulated data, which comprised 100 two-dimensional vectors (see Fig. 4*A*). Vector components for the first 50 simulated trials were randomly distributed in the interval (0, 1) with variance = 0.1. Vector components for the next 50 trials were randomly distributed in the intervals [(0, 1), (0.5, 1.5), (1, 2), (2, 3), and (4, 5)] with variances = 0.1; i.e., the distance between mean motor patterns of the first and second 50 trials was successively increased. Because the distance was increased, the number of trials that belonged strongly to one or another cluster, i.e., with membership grades of >0.85 based on a 0.0–1.0 scale, increased (see Fig. 4*A*). With minimal overlap between the first and second 50 trials (distance = 1.0), FCM strongly clustered 75% of trials into one or the other cluster. Thus, we considered 75% a target percentage for "good" clustering. We specified different numbers of clusters for our IC activation patterns (two to five) to see which cluster number provided the best clustering (>75%). We also performed FCM using an additional 10 parameters that described the timing of peak IC activation, e.g., 100 twenty-dimensional vectors.

Single-cell activity patterns were discriminated from raw stereotrode data used custom-written software (Matt Wilson). M1 cells were distinguished primarily on the basis of the relative amplitudes of their spikes on the two stereotrode wires (Poe et al., 2000). As many as five or six cells could be identified and isolated on one stereotrode with a cluster-cutting technique. This method involves extraction of a set of spike waveform parameters (mainly spike height and width) for each spike from the two stereotrode channels and the separation of units on the basis of these parameters using interactive graphics software. Different combinations of parameter pairs were projected as two-dimensional scatterplots. When this was performed, points derived from single cells tended to form recognizable clusters. The spikes within a cluster were enclosed in a polygon drawn using the computer mouse. The data points were then projected into new two-dimensional plots in which the earlier partitions of the data were preserved by color coding the points lying within the polygon boundaries. This process was performed until a multidimensional set of boundaries was established that provided the subjectively best separation of spike waveform clusters. The times of spikes in each cluster (or for each cell) were exported to Matlab for analysis.

In Matlab, perievent histograms (PETHs) of cell spike times were computed relative to the instant of pellet contact (±4 sec). All reach trials (e.g., 100 trials) were aligned at pellet contact to generate a data array, e.g., 100 rows × 4000 columns. PETHs were computed in 20 msec bins (or columns) and expressed as a rate (spikes per second) or probability. A three-point boxcar filter was used to smooth PETHs. Significant changes in the peak amplitude, time of peak, and integrated area of PETHs between blocks were determined using paired *t* tests.

Linear cross-correlations were performed using the Matlab system identification toolbox m-file cra($Z$,$M$) where $Z = (y\ u)$, $u$ is the input signal, $y$ is the output signal, and $M$ is the number of lags (±750 msec) for which the cross-correlation function between $u$ and $y$ was computed. Cross-correlations were computed between low-pass-filtered (five-point Gaussian; moving time window, 5 msec) PETHs ($u$), rectified, filtered EMGs ($y_1$), and IC activations ($y_2$). A shift predictor correction was determined by computing cross-correlations between $u$ and time-shifted $y$ values (e.g., shifted by $1 * 4$ to $N * 4$ sec, where $N$ is the number of trials, and 4 is the length in seconds of each trial (±2 sec relative to pellet contact; for more thorough description of the shift predictor, see Miller et al., 1993). Significant cross-correlations (at $p < 0.05$) were determined by assessing whether peaks or valleys of the original cross-correlation were ±2 SD outside the mean shift-predicted correlation in the functionally important time window of +150 msec; i.e., we looked for correlations with positive lags (see shift predictor example in Fig. 1*C*). A causality $u \rightarrow y$ would result in a positive lag. However, we recognized that positive lags do not necessarily imply causality $u \rightarrow y$.

Videotaped reaches were analyzed off-line by transferring digital video to a hard disk and by importing video frames into Matlab. The approximate positions of the base of the fingers, wrist, elbow, and shoulder joint centers were digitized from the lateral view. We determined the wrist, elbow, and shoulder angles and the trajectory of the hand (velocity and position) for each of these trials. The normalized path distance of the hand to the pellet was computed as described by Kargo and Giszter (2000b); this is a measure of curvature of the hand path. We tested for significant differences in starting limb position, limb position at tray contact, peak hand velocity, and normalized path length across blocks on the first day. From the top view, we determined and tested for differences in the length of time spent on the tray and finger spread (distance between the tips of the first and fourth digits) on tray contact.

## Results

### Behavioral evidence for early skill learning

On the first day of skill training, animals displayed fast, within-day improvements ($n = 11$ animals). Animals also displayed more gradual, across-day improvements. Each day's training session was divided into three successive blocks with equal numbers of attempts per block. On day 1, success rates increased from 38 ± 5% (SD) in the first block to 54 ± 8% in the last block (16% increase per ~120 attempts). All rats increased success rates from the first to last blocks on day 1. Systematic within-day increases were not observed on later days, but interday success rates still increased gradually from 45 ± 9% on day 1 to 75 ± 5% on day 10 (30% increase per 1200 attempts). Thus, these data support at least two stages of skill learning, early and later, more gradual learning. Below, we focus on EMG mechanisms underlying the early stage (day 1) and its M1 correlates.

### Early skill learning was expressed through two general mechanisms

Success rates improved potentially for one of two reasons: either the probability of activating motor patterns that succeeded versus

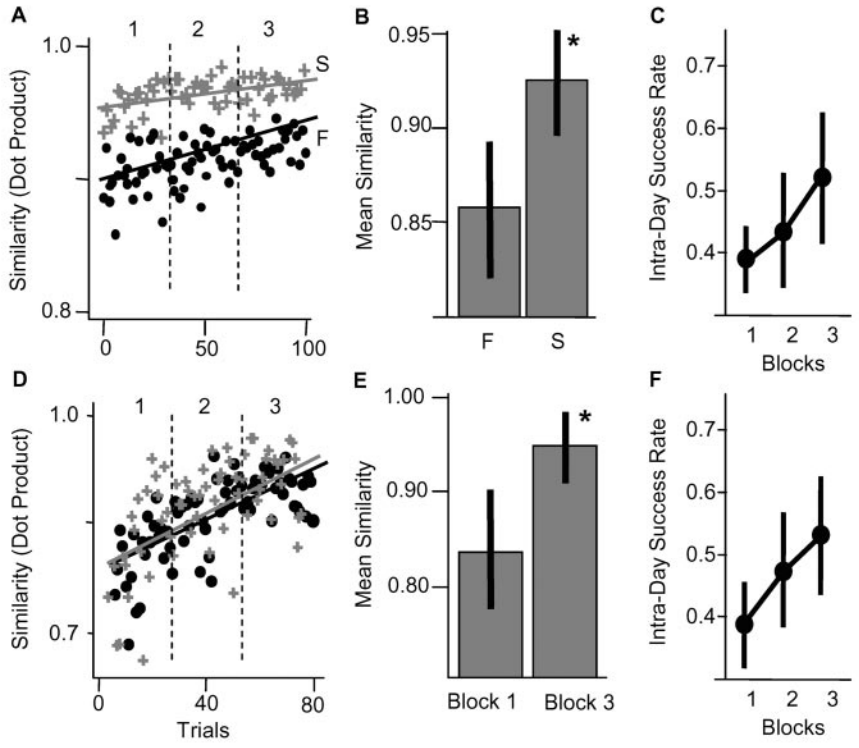


**Figure 2.** Evidence for two early learning strategies. *A, D*, Similarity values between motor patterns of individual trials (up to pellet contact) and the mean successful pattern of block 3 (plus signs, successes; circles, failures, left-to-right trial numbers, 1–3 denote trial blocks). *A*, Similarity values in rat K organized into two groups, one associated mainly with successes and another associated with failures. *B*, In 3 of 11 animals (including rat K), failure motor patterns were significantly less similar compared with successful patterns ( $p < 0.01$; mean ± SD shown). *C*, Success rates for these three animals across blocks. *D*, In rat E, similarity values for success and failure motor patterns overlapped throughout training. *E*, In 8 of 11 animals (including rat E), motor patterns activated in Block 3 were significantly more similar to the mean successful pattern of Block 3 than were patterns activated in Block 1 ( $p < 0.05$). *F*, Success rates for these eight animals.

ones that failed increased, or the probability of success of a single motor pattern increased over time by tuning the pattern. To test these possibilities, we calculated the similarity between the motor pattern of each trial and the mean successful pattern for the last block (see Materials and Methods). We reasoned either that successful patterns would be fundamentally different than failures, and so similarity measures would cluster into distinct groups (selection), or that motor patterns later in the day would be different than the initial patterns, and so similarity measures would incrementally increase over the day (tuning).

Skill improvement was associated with both motor pattern selection and pattern tuning. One group of animals (3 of 11; rats D, K, and L) appeared to switch between motor patterns underlying the reach portion of the task. Figure 2*A* shows data for rat K. Each point is one trial (black, failures; gray, successes) and represents how similar the motor pattern of the trial was to the mean successful pattern of block 3. Similarity measures were averaged across the reach duration; reach duration was the period from 50 msec before reach onset up to the time of pellet contact (~280–380 msec). Reach onset was defined as the onset of the deltoid (clavicular head) EMG burst, which preceded limb advancement to the pellet by 16.67–50 msec (as determined from video in three animals) and which was reliably activated in all animals an average of 302 ± 18 msec before pellet contact. Measures of motor pattern similarity during this period separated into two groups associated with either failure or success. The combined mean similarity for failed motor patterns was significantly less than that for successes in these three animals [Fig. 2*B*, failures (F), 0.85 ± 0.05 (SD); successes (S), 0.93 ± 0.04; significant at $p < 0.02$].

In contrast to the first group of animals, a second group (8 of 11; rats E, G, I, M–P, and R) appeared mainly to tune a single starting motor pattern over time. Figure 2*D* shows data for rat E. Similarity measures for failed and successful motor patterns overlapped and did not cluster into separate groups; the same 10 muscles were recorded in rat E as in rat K. For this second group, we found that all motor patterns activated in the first block were significantly less similar to the mean successful pattern of block 3 compared with all motor patterns activated in the last block, which indicates changes in the motor pattern over the day (Fig. 2*E*; Block 1, 0.83 ± 0.07; Block 3, 0.94 ± 0.04; significant at $p < 0.02$).

The two groups of animals did not differ significantly in the level of skill improvement on day 1 (Fig. 2*C,F*). The selection group (3 of 11) started at a success probability of 0.38 ± 0.04 in block 1 and finished at 0.52 ± 0.10 in block 3. The tuning group (8 of 11) started at a success probability of 0.39 ± 0.06 in block 1 and finished at 0.55 ± 0.09 in block 3.

Similarity measurements for postcontact motor patterns (after pellet contact) always separated into distinct success and failure groups. Combined means for all animals were significantly different at $p < 0.001$ (failures, 0.65 ± 0.12; successes, 0.92 ± 0.08). The striking difference in postcontact patterns was attributable to the finding that if the hand was inappropriately targeted or oriented at pellet contact, the grasp and retraction phases of the motor pattern were not activated or weakly activated, or a new reach was initiated. Thus, although it is possible that improved success rates were attributable to an increased probability of activating muscles more appropriately after pellet contact, the main mechanism for skill improvement probably was attributable to either selection or tuning of precontact motor patterns.

Below, we examine whether selection and tuning of muscle activation patterns occurred with respect to motor programs (sequences of synergistic contractions), individual synergies, or individual muscles. To examine these possibilities, we used ICA to extract underlying synergies from the EMG data (see Materials and Methods).

### Motor program selection

The selection group of animals appeared to switch between the activation of different motor programs, where motor program refers to a specific sequence of synergy activations or of independent components (ICs). Figure 3 shows the activation pattern of seven ICs in rat D. These seven ICs accounted for 83% of the EMG variance during reaching (10 muscles recorded). IC activations are shown from trial to trial [Fig. 3, left columns; each row is one trial; only the first and last 10 failures (F) and successes (S) are shown, and red represents regions of highest IC activity].

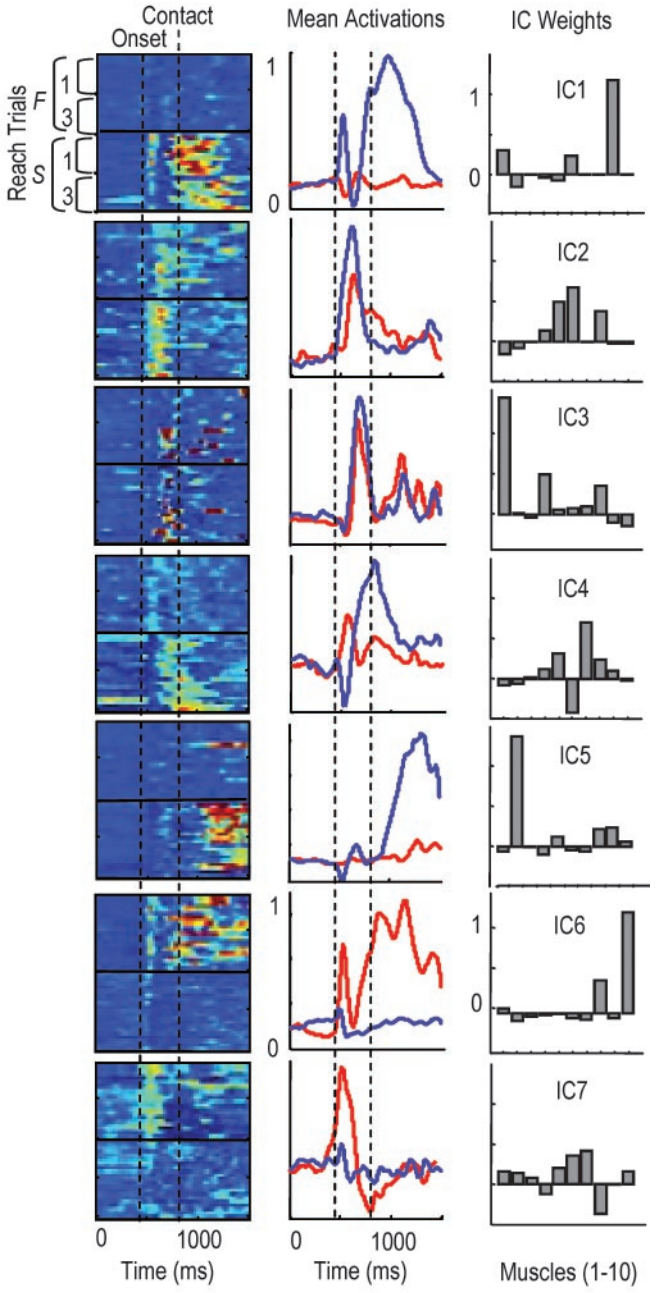


**Figure 3.** Evidence for motor pattern switching during early learning. Left column, Activation of ICs over time as contour plots (each row is 1 trial). Red, Regions of highest activity (normalized to 1.0); blue, regions of lowest activity (0). First vertical line, Approximate reach onset; second line, time of pellet contact. The first and last 10 failures (F 1, 3) and 10 successes (S, 1, 3) are shown. Middle column, Averaged IC activations for failures (red) and successes (blue). Right column, Bar plots showing IC weights (muscles from left to right: lateral triceps, biceps, pectoralis, medial triceps, deltoid, trapezius, FCU, ECU, ECR, brachialis). The first five rows show ICs activated strongly during successes: IC1, associated with initial hand supination; IC2, limb advancement; IC3, limb extension and hand positioning before contact; IC4, grasping; IC1, supination; IC5, retraction. The last two rows show ICs activated more strongly during failures: IC6, elbow flexion and wrist extension; IC7, limb advancement.

Middle columns show averaged IC activations (red, failures; blue, successes). In both the left and middle columns, the period between the vertical bars represents the time window over which the reach to the pellet occurred, which is the period in which switching occurred. The period after the second vertical line represents the time window of pellet contact, grasping and limb retraction. Right columns show the manner in which ICs were distributed to forelimb muscles; these are the IC weights. In rat D, IC1 was strongly activated to start most successful attempts and was followed by activation of ICs 2–5. IC1 was only weakly activated during failed attempts (Fig. 3, top row). In contrast, IC6 and IC7 were strongly activated to start most failed attempts and were followed by activation of IC2, IC4, and then IC3. IC1 was distributed to lateral triceps, trapezius, and ECR, whereas IC6 was distributed mainly to brachialis and ECU.

To examine more thoroughly the observation of motor pattern switching, which occurred before pellet contact, we performed FCM of IC activation patterns to attempt to group patterns into specific clusters (see Materials and Methods). The precontact activation pattern of each trial was described by the set of peak IC activations that occurred before pellet contact (e.g., a four- or five-dimensional vector). To evaluate the FCM goodness of clustering, we simulated two-dimensional motor patterns (a1 and a2), where a1 and a2 represent peak activations of virtual ICs (see Materials and Methods). Figure 4*A*, top three graphs, shows three different 100-trial simulations in which the mean distance between two different motor patterns (filled, open symbols) was progressively increased (diamond, overlapping motor patterns; circle, mean distance between motor patterns = 0.5; square, mean distance = 1.0). The bottom graph shows the percentage of trials for each simulation run that were classified as belonging strongly to one or another motor pattern cluster, i.e., membership function >0.85. When the two motor patterns were not overlapping in the activation space (filled squares, distribution of motor pattern 1; open squares, distribution of pattern 2), FCM classified ≥75% of the trials as belonging strongly to one or another cluster, i.e., FCM >0.85. Thus, we considered 75% a baseline measure for FCM goodness of clustering.

Figure 4*B*, top graph, shows the distribution of membership functions for rats D (black) and E (gray), animals that respectively did and did not appear to exhibit switching. Seventy-five percent of trials (150 of 200) in rat D were strongly clustered into one or another motor pattern type (75% of FCM values >0.85). In the three animals exhibiting switching, 77 ± 12% (SD) of trials were strongly clustered into two pattern types (Fig. 4*B*, bottom graph, black). Specification of three or more clusters reduced the goodness of clustering (Fig. 4*B*, bottom graph). This suggests that these animals switched mainly between two pattern types. In contrast to rat D, only 12% of trials (17 of 140) in rat E were strongly clustered (Fig. 4*B*, top graph, gray line). In the eight animals not exhibiting switching, only 18 ± 8% of trials were strongly clustered (Fig. 4*B*, bottom graph). Even when temporal parameters were included in the data vector describing the pattern of each trial (e.g., IC1 amplitude . . . ICN amplitude, IC1 onset time . . . ICN onset time), only 19 ± 9% of trials were strongly clustered in these eight animals. Thus, motor patterns occupied an overlapping region of the activation parameter space and therefore formed a single pattern type.

Different motor pattern clusters had different probabilities of success. In rat D, 72% of motor patterns belonging to cluster 1 were successful (i.e., patterns with membership grades of >0.85). Only 18% of motor patterns belonging to cluster 2 were successful. In each of the three animals exhibiting switching, one cluster had a higher probability of success (68 ± 7%) compared with the other cluster (21 ± 9%). Importantly, the probability of activating motor patterns that had the higher probability of success increased over the first day of training and accounted in part for the improved success rates (block 1 probability of activating successful cluster, 40 ± 8%; block 2, 48 ± 10%; block 3, 57 ± 8%).

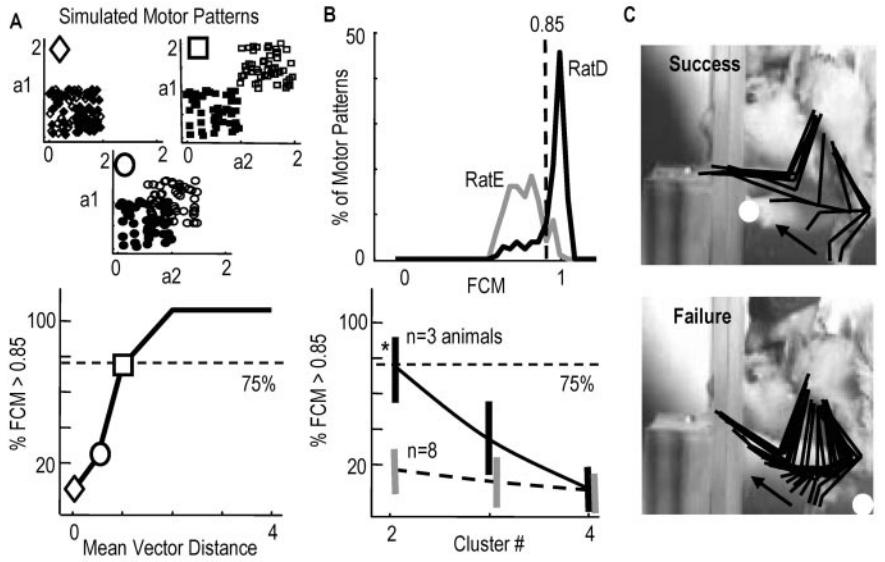


**Figure 4.** Quantification of motor pattern switching during early learning. *A*, Simulated data to assess goodness of clustering by the fuzzy c-means algorithm (FC; see Materials and Methods). Top graphs, Two motor patterns with different means and equal variance (0.1) were simulated (filled, unfilled symbols, respectively; a1, a2, activations of two actuators on any one trial; diamonds, equal means; circles, mean difference = 0.5; squares, mean difference = 1.0). When the two patterns were nonoverlapping (squares), FC assigned 75% of the simulated trials (200) to one or another motor pattern cluster, i.e., 75% of FCM functions >0.85. *B*, Top graph, Distribution of FCMs for ratD (black) and ratE (gray). More than 75% of FCMs were >0.85 in ratD; only 12% were >0.85 in ratE. Bottom graph, Goodness of clustering for three animals exhibiting switching (black) and eight animals not exhibiting switching (gray). More than 75% of FCMs were >0.85 in the three animals when only two clusters were specified. Goodness of clustering was reduced when more (3 or 4) clusters were specified. C, Representative kinematics of forelimb during failure (bottom) and success (top) in rat D, shown at 16.67 msec intervals; white dots, position of contralateral hand; arrows, direction of ipsilateral hand movement.

Switching between motor patterns depended in part on the initial posture of the animal. On failed reaches, rat D had an increased probability of starting the reach with the contralateral hand on the ground (83 of 114 or 73% of failed attempts). In contrast, on successful reaches, rat D had an increased probability of starting the reach with the contralateral hand supported against the wall (64 of 84 or 76% of successes). The probability of placing the contralateral hand against the wall before reach onset increased over time (40% first block and 55% last block). This was correlated with an increased probability of success (32% first block and 50% last block) and with an increased probability of activating motor patterns belonging to the more successful cluster. Rats K and L showed a similar dependency on initial posture, but the specific postural dependencies varied. Rat K activated one motor pattern more often when the longitudinal body axis was parallel to the aperture (59 of 85 or 70% of failures) and a different motor pattern when the body axis was at an acute angle to the aperture, which forced reaching across the chest and a different starting pattern of hindlimb–contralateral forelimb support (49 of 65 or 75% of successes). Rat L showed a dependency on whether reach onset occurred solely with hindlimb support (70 of 85 failures) or with tripedal support (hindlimbs and contralateral forelimb; 40 of 61 successes).

There were obvious functional differences associated with switching between motor patterns and starting the reach from different postures. In rat D, the final position of the hand (wrist joint center) at the time of tray contact differed significantly between failures and successes: in failures, the wrist was –5.2 ± 2.5 (SD) mm relative to the pellet location; successes, –1.8 ± 2.5 mm (see representative digitized reaches in Fig. 4*C*). The inappropriate targeting of the hand to the pellet was common to all three animals and consistent with activation of different motor patterns to start the reach: significantly short of the pellet (two of three animals) or medial to the pellet (i.e., the arm was overly adducted in one of three animals) in failed attempts compared with successful ones.

Activity patterns in motor cortex (M1) well before reach onset provided information about subsequent behavioral performance in these animals. Discriminant analysis of M1 activity patterns was performed to assess whether and when behavioral performance could be predicted (11 M1 cells in rat D, 14 cells in rat L, and 5 cells in rat K). Figure 5*A* shows mean activity patterns of the ensemble across time in rat D; the top panel is the successful pattern, and the bottom panel is the failure pattern. Each row represents firing rates of one cell across time [white is highest firing rate (40 Hz), black is lowest rate (0 Hz)]. Behavioral performance was predicted significantly above chance at relatively early times before reach onset (Fig. 5*B*; data from the three animals). The maximum prediction rate was 80 ± 4% (SD) during the 0.5–1.0 sec before reach onset. Prediction rates increased at reach onset to 90 ± 7% and to 93 ± 5% at pellet contact. The ability of prereach M1 activity to predict performance was related to its ability to predict motor pattern selection. The maximum prediction rate was 83 ± 5% (for predicting activation of motor patterns belonging to one or the other cluster, which had different probabilities of success). In contrast, in the other eight animals that did not show evidence for motor pattern switching, maximum prediction rates of behavioral performance were significantly above chance only near the time of pellet contact (92 ± 6%; see data from two representative animals in Fig. 5*C*; rat R, 20 cells; rat M, 8 cells).

The ability of prereach muscle activity patterns to predict behavioral performance was above chance (maximum of 71 ± 6% from 0.5 to 1.0 sec before reach onset) but considerably lower than prereach M1 activity patterns. Similarly, prereach IC activation patterns (usually the activation amplitude of one posture-related IC) were less effective than M1 patterns in predicting behavioral outcome (71 ± 5%). The 10% difference in prediction capabilities before reach onset might be attributable to M1 receiving proprioceptive feedback in addition to driving postural muscle activity.

### Adaptation of synergy composition

The majority of animals did not show evidence for switching between motor patterns on day 1 ($n = 8$). These animals appeared to activate a similar motor pattern for both failed and successful attempts and adjusted this motor pattern gradually over time to increase its probability of success, i.e., motor patterns later in the day were less similar to starting patterns. We examined the substrate for this tuning.

Every animal ($n = 11$) showed evidence for adapting the composition of muscle synergies with training, where synergy composition refers to the IC weights. IC weights represent how an

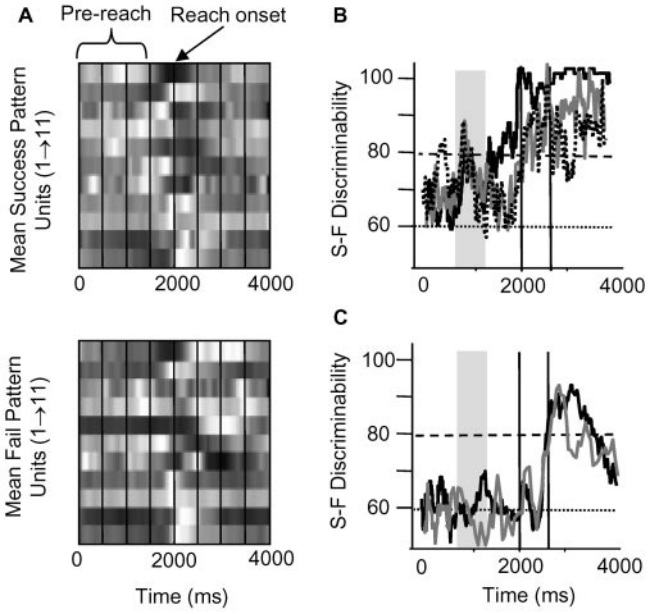


**Figure 5.** Prereach M1 activity predicts performance in animals exhibiting motor pattern switching. *A*, Top panel, Mean pattern of M1 activity during successful reach in rat D. Bottom panel, Mean pattern during failed reach. Each row represents the firing rate of one M1 cell over time. Firing rates were normalized from 0% (black) to 100% (white) of the maximum firing rate in the ensemble ($n = 11$ neurons). Vertical lines, 500 msec intervals, and reach onset occurred at 2000 msec. Different temporal modulations of M1 firing occurred between success and failure trials. *B*, Discriminant analysis showed that firing patterns predicted significantly above chance behavioral success and failure. Discriminant analysis was performed −2 to +2 sec relative to reach onset. In three animals exhibiting motor pattern switching, the maximum predictive ability of M1 patterns before reach onset approached 80%, a full 1 sec before reach onset (gray bars, times 1200–800 msec before reach onset). Predictive ability increased at reach onset (first vertical line) to 85–100% and increased further at pellet contact (second vertical line) to 90–100%. *C*, Discriminant analysis in animals not exhibiting switching showing that M1 patterns predicted performance above chance only at the time of pellet contact. Data for two animals are shown (rat M, 8 units; rat R, 20 units).

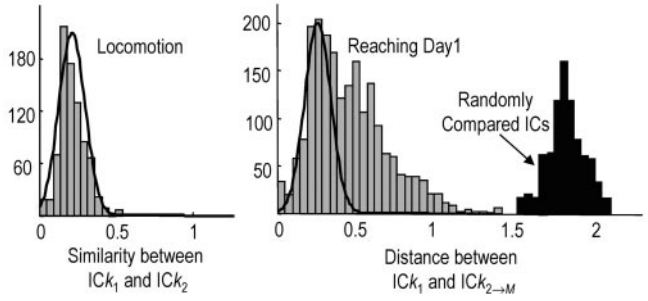


**Figure 6.** Muscle synergy composition was adapted during early learning. Left graph, Bar plot of Euclidean distances between the weights of most similar ICs, which were extracted from separate lap-running sessions in five animals [*k*, IC number (e.g., 1–6); 1, 2, lap sessions). The distribution was unimodal. Right graph (gray bars), Distribution of Euclidean distances between the weights of reaching ICs extracted during the first 10 attempts (segment 1) and the weights of most similar ICs extracted during later 10-trial segments (M, last segment; 8 animals). This distribution was bimodal. One group of values had a similar distribution as the locomotor data (normal fits of locomotor data are scaled and superimposed). A second group was outside the locomotor range. Black bars, Distribution of distances between the weights of randomly compared reaching ICs ($n = 4$ animals). These data were much farther outside the range of locomotor values.

(estimated) source signal was distributed to coactive muscles. This distribution pattern might be invariant or adaptable. To test this, we first compared the weights of ICs that were extracted from two locomotor sessions (see Materials and Methods). We hypothesized that weights for muscle synergies activated during locomotion should be invariant across time. The Euclidean distances between the weights of the most similar locomotor ICs (from running sessions 1 and 2) formed a single distribution with a mean of 0.22 ± 0.10 (SD) (Fig. 6, left-most graph, combined data for five animals); the mean dot product between the weights of most similar ICs was 0.96 ± 0.04. The most similar ICs were those that had the smallest distance between the vector of IC weights (see Materials and Methods). We then applied ICA to *M* successive overlapping segments of reaching trials in individual animals (e.g., trials 1 → 10, 2 → 11 . . . *N*–9 → *N*, where *N* is the last trial) and compared the weights of the most similar ICs in the first segment and all later segments. In contrast to the locomotor data, distance values for reaching ICs formed two groups (Fig. 6, middle graph, gray bars, combined data for eight animals). One group of distance values overlapped with the locomotor data. Thus, the weights of some reaching ICs were mostly invariant with training. A second group of distance values was outside the range of the locomotor data. The mean Euclidean distance for this second group was 0.67 ± 0.31; the mean dot product between weights in this second group was 0.75 ± 0.21 (compared with 0.96 ± 0.04 for locomotor pairs), which indicates that the balance of muscle activations within an IC was considerably more variable during the initial reach training.

Two observations further support the idea that IC weights were adapted or fine tuned with training, in contrast to activating completely new ICs with training. First, distance values for randomly compared IC pairs, i.e., those that were not the most similar from reach segment to segment, were much farther outside the locomotor range (Fig. 6, black histogram bars) compared with the most similar reaching IC-pairs. Second, most similar reaching ICs had the same onset time and time of peak activation across reaching segments. In summary, many source signals appeared to have similar time courses of activation over the day, and mainly the weights (or distribution patterns) were changed with training for specific source signals.

In individual animals, the weights of only specific ICs were adapted during training. To demonstrate this finding, we describe a result that was common in the majority of animals. Six of 11 animals showed specific changes during training in the weights of an IC that was activated ~100–150 msec before pellet contact. This IC was distributed primarily to wrist and extrinsic finger muscles. We referred to this IC as a "hand-related" IC. Figure 7*A*, left column, shows the activation patterns of five ICs, which accounted for 71% of the EMG variance in rat E (black lines are averaged activity for the 54 trial segments, and each row represents IC activity for one trial segment). The fourth IC from top was the hand-related IC. IC weights for the first trial segment are shown in the middle column; IC4 was distributed initially to the extrinsic hand muscles FCU, ECU, and ECR. IC4 weights changed during training. That is, similarity values between the initial IC4 weights ($IC4_1$) and IC4 weights on later trial segments ($IC4_{2 \rightarrow M}$, where M is the number of trial segments) were >1 SD away from the mean distance between most similar locomotor ICs [Fig. 7A, right column; the mean locomotor distance was 0.22 ± 0.10 (SD)]. The other four ICs were stable over the day, i.e., within 0.22 ± 0.10. Specific changes to the muscle balance within IC4 are shown in Figure 7B (blue, FCU; red, FCR; black, ECU). The balance of spatially coherent activity was shifted so that wrist–finger flexors (FCR and FCU) were activated more strongly during this coherent burst of activity; ECU activation

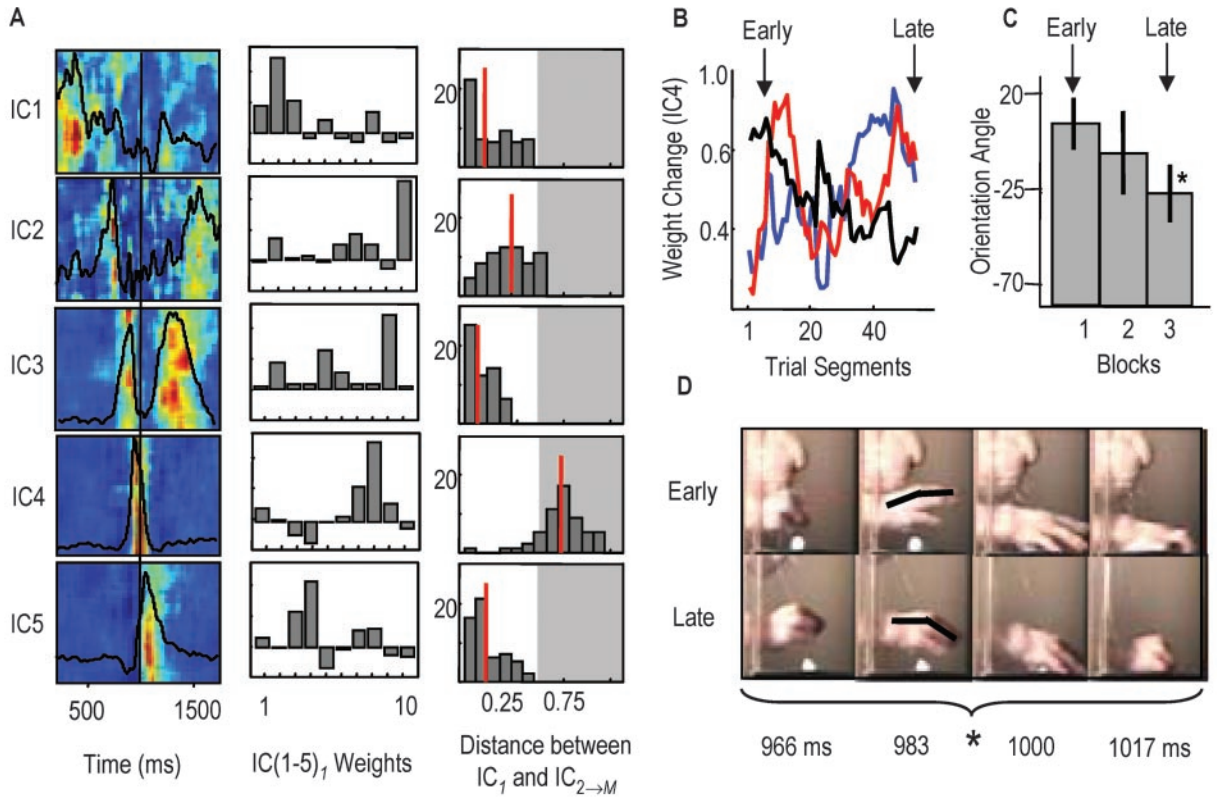


**Figure 7.** Adaptation of hand-related synergies during early learning. *A*, (similar format as Fig. 3), Contour plots showing the activation pattern of five ICs; each row is one attempt (65 attempts total); red, highest activity. Mean activations are superimposed (black lines). Bar plots in the middle column show IC weights for the first 10 trials (muscles from left to right: lateral triceps, biceps, teres major, FCR, deltoid, trapezius, FCU, ECU, ECR, brachialis). ICs were activated sequentially through time (top to bottom: IC1 associated with prereach posture; IC2, limb flexion; IC3, reach onset; IC4, elbow extension, hand positioning; IC5, grasping. Bar plots in the right column show the distribution of Euclidean distances between $IC_1$ weights and $IC_{2\rightarrow M}$ weights, where 1 refers to trials 1–10; 2, trials 2–11, and M, last 10-trial segment. Red lines, Mean distance between initial and later IC weights. Only IC4 weights were significantly changed during training (i.e., $>0.22 \pm 0.10$, see Results, Adaptation of synergy composition). *B*, Specific changes to IC4 weights across the day (blue, FCU; red, FCR; black, ECU). The balance of activity was shifted so that during block 3, wrist–finger flexors were activated more strongly within this burst of activity. *C*, The orientation angle of the fingers (relative to horizontal) was reduced from block 1 to block 3. *D*, Four consecutive frames of the hand during early and late reaches (in 16.67 msec intervals). Notice that the orientation angle of the fingers was reduced in the later reach.

was reduced, whereas ECR activation remained unchanged (data not shown).

The finding that IC4 composition was specifically changed without changing either the composition of other synergies or the basic motor pattern (i.e., the sequential and partly overlapping pattern of IC activations) suggests that functional changes might have been produced solely through IC4 adaptation. One observed change was a reduced finger extension angle, on entry through the aperture, over time [Fig. 7*D*, top row, early (5th) reach, bottom row, late (50th) reach]. Comparison of the orientation angle of the digits relative to horizontal for the first and last 20 reaches revealed a significant decrease over time [Fig. 7*C*, Block 1, $5 \pm 10°$ (SD); block 3, $-30 \pm 12°$]. This reduced extension was correlated with a reduced delay between reach onset and pellet contact (first 20 reaches, $305 \pm 15$ msec; last 20 reaches, $272 \pm 13$ msec). Most importantly, these functional changes in hand–finger kinematics and contact times were correlated with increased success rates over time (first block, 40%; last block, 52%).

We next examined M1 correlates for synergy adaptation. First, we examined generally whether M1 activity was related to IC activations across time. Second, we cross-correlated the firing rates of individual M1 cells with muscle and IC activations to quantify this relationship. Last, we examined whether coactive M1 cells, which were correlated with the same adaptable IC, were regulated differently with training (see Materials and Methods; rat D, 11 cells; E, 8; I, 2; K, 6; L, 14; M, 8; N, 1; O, 5; P, 3; R, 20; and S, 22).

The mean firing rates of M1 cells were closely related, with appropriate time delays, to the mean activation patterns of specific ICs. Figure 8 shows data for rat L. Each graph shows the mean firing rate of one cell (black) and mean activation of the corresponding IC (gray) to which each cell was significantly correlated (correlations after subtraction of the shift predictor are shown to the right of each graph). M1 cells and the corresponding ICs were activated in a sequential and partly overlapping manner through time (top to bottom). ICs were named in Figure 8 to correspond to the function of the activated muscles and the time-matched kinematics: an initial postural IC (often tonically activated; muscles FCU, triceps group, and trapezius), an initiation IC (begins the reach to the pellet; deltoid, brachialis, biceps, and pectoralis major), a hand-related IC (activated during transport to the pellet; lateral triceps, ECU, ECR, and FCR), a grasp IC (activated at pellet contact; FCU, FCR, ECU, deltoid, and medial triceps), and a retraction IC (retracts forelimb; biceps, teres major, ECU, FCU, and brachialis). Muscles activated by these five ICs were generally consistent among animals.

Firing rates of M1 cells were positively correlated most often with the activation patterns of multiple muscles across the 4 sec trial period ($\pm 2$ sec relative to pellet contact) but primarily with

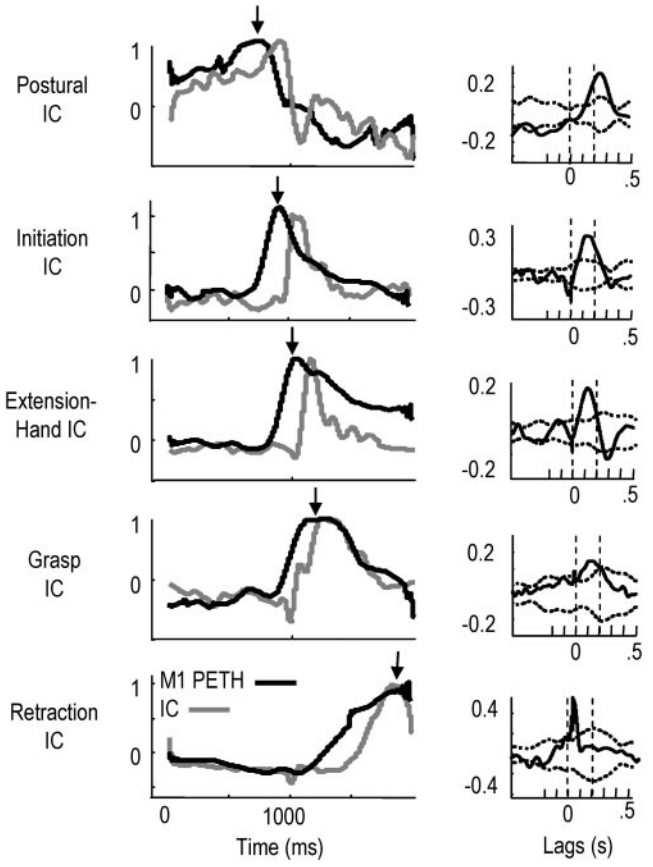


**Figure 8.** M1 firing rates were related to the mean activation pattern of ICs during the reach. Left column, Black lines, Mean firing rates of different M1 neurons in rat L (mean of 40 successful reaching trials, each normalized to 1.0); gray lines, IC activations to which the corresponding cells showed significant positive cross-correlations. The cross-correlations are shown in the right columns [black, cross-correlation computed at lag times of −500 to +500 msec; dotted lines, 95% confidence interval for the shift-predictor cross-correlation (see Materials and Methods)]. M1 neurons and ICs were activated in a sequential and partly overlapping manner during the task. The ICs shown here were distributed to similar muscles between animals: IC1 (prereach posture), FCU, triceps muscles, and trapezius; IC2 (reach initiation), deltoid, brachialis, and biceps; IC3 (limb extension, hand shaping), lateral triceps, ECU, and ECR; IC4 (grasping), FCU, FCR, medial triceps, and deltoid; IC5 (retraction, supination), biceps, teres major, ECU, and brachialis.

the activation of only one IC. The percentage of M1 cells that had significant positive cross-correlations (in the functionally important time window of 0–150 msec) with both muscles and ICs, after correcting correlations with the shift predictor (see Materials and Methods), was 37% (37 of 100 cells). The mean peak correlation of these 37 cells with muscle activations was 0.29 ± 0.04 (SD). The mean lag at which peak correlations occurred was 62 ± 18 msec. These cells were correlated with an average of 3.5 ± 1.3 forelimb muscles. The mean peak correlation for these same cells and IC activations was 0.20 ± 0.05. In contrast to M1 correlations with multiple muscles, M1 cells were correlated with only 1.19 ± 0.40 ICs (30 cells correlated with only one IC, and 7 cells correlated with two ICs). Individual cells were not usually correlated with all muscles constituting an IC to which it was also correlated. That is, computed ICs had an average of 5.25 ± 2.32 muscles with positive weights (i.e., that received excitation), whereas the averaged cell was positively correlated with only 3.51 ± 1.36 muscles. In addition, M1 cells were not usually correlated with muscles in the IC that had negative weights (i.e., that did not receive excitation from the source signal). M1 cells were positively correlated with only 0.81 ± 0.50 muscles that had negative weights within the IC to which the cell was also correlated.

In summary, 37% of M1 cells were positively correlated with specific IC activations. Cells were positively correlated with most muscles that were activated by the IC but not all muscles. Cells correlated with an IC were not usually correlated with muscles that were not activated by the IC. We focus our analysis below on these 37 cells, which had positive correlations with multiple muscles and primarily one IC.

Coactive M1 cells, which were correlated with the same adaptable IC, were often regulated differently during training. That is, the peak firing rates of M1 cell pairs were either increased or decreased in parallel during training but in a disproportionate manner or were oppositely affected (e.g., increases in one and decreases in the other). Figure 9*A* shows spike cross-correlograms for three cells in rat L (shown as the probability of spiking in 20 msec bins). Cross-correlograms for cells n10 and n11 were performed with respect to cell n03. The third cross-correlogram for n11 was performed with respect to n10. Cells n10 and n11 had significantly correlated activity with n03, and cell n10 had correlated activity with n11 ( $p < 0.05$; 95% confidence interval shown in Fig. 9*A*). The times of peak firing in these three cells were constant over the day [n03, 905 ± 15 (SD) msec; n10, 921 ± 13 msec; n11, 897 ± 21 msec]. However, the peak rates changed differently; e.g., the ratios of firing (n03: n10: n11) started at 1.00:1.12:2.25, changed to 1.00:1.00:0.64 at midday, and ended at 1.00:0.92:0.38 (Fig. 9*B*).

Each of the above three cells had firing rates that were significantly correlated with the activation of similar but different sets of muscles (Fig. 9*C*; peak correlations within the 0–150 msec time window are shown between each cell and each muscle; asterisks mark significant correlations). All cells were correlated with lateral triceps (muscle 4) and deltoid (muscle 5); cells n03 and n10 were correlated with trapezius (muscle 6) and brachialis (muscle 10); and cells n10 and n11 were correlated with biceps (muscle 2). Each cell was also correlated with the same IC (initial weights for this IC are shown in Fig. 9*D*, top). The weights for this IC were adapted with training (Fig. 9*D*, bottom, dark gray, brachialis activity was increased; black, deltoid was increased and then decreased; light gray, trapezius was decreased). Cells n03 and n10 were both correlated with trapezius and showed reduced firing rates over time, consistent with a reduction in trapezius weights over time. Cell n11 was correlated with biceps and showed increased firing rates over time, consistent with increases in biceps weights over time.

In 7 of 11 animals, there was at least one M1 cell pair on the first day of training that had correlated spiking activity (i.e., wherein there was a significant increase in the probability of spiking when the other cell spiked at $p < 0.05$). There were 11 total cell pairs. We calculated the mean (peak) firing rate of cell pairs in the first, second, and last blocks of reaching trials and assessed whether both cells showed significant increases, decreases, or no change in peak firing rate over the day. Of the 11 pairs (3 in rat D, 3 in rat L, 1 in rat E, 1 in rat M, 1 in rat O, 1 in rat P, and 1 in rat R), 6 showed different patterns of regulation during training; i.e., one cell had significantly increased, and the other had significantly decreased or no change in peak firing rate. Five of 11 cell pairs had the same pattern of regulation, i.e., either no change in both or significant, proportionate increases or decreases in firing rate. Thus, these data provide some evidence that certain coactive M1 cells were correlated with the same synergistic pattern of muscle activation and that fine tuning the balance (or ratios) of

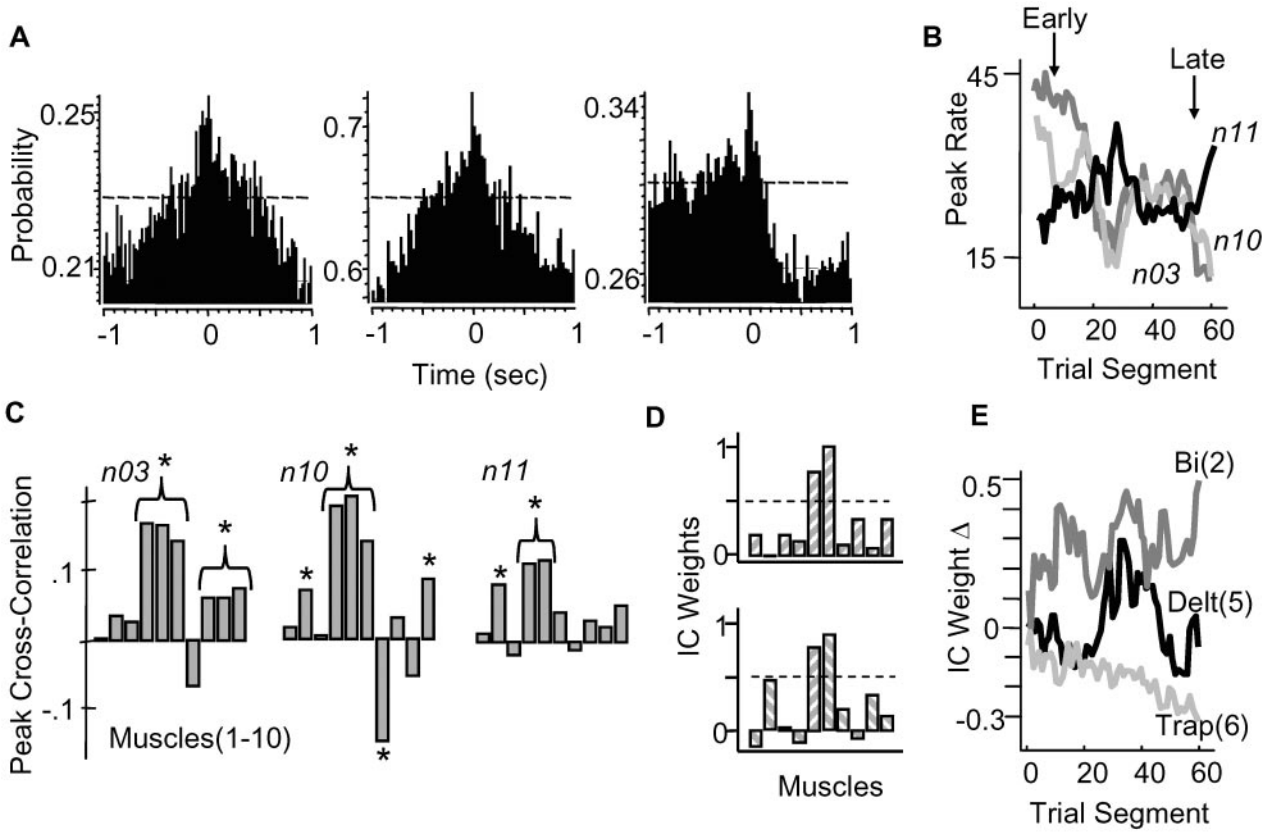


**Figure 9.** The firing rates of coactive M1 cells could be regulated differently with training. *A*, Cross-correlations between spiking activity of three coactive M1 neurons (n03, n10, n11) in rat L, represented as probability of spiking in 20 msec bins. Cross-correlations in the middle and right panels were performed with respect to n03 (for cells n10, n11); cross-correlation in left panel was performed with respect to n10 (for cell n11). Each cell had significantly increased probabilities of spiking when a spike occurred in another cell (95% confidence interval shown). *B*, Peak firing rates changed disproportionately with training (dark gray, n03; light gray, n10; black, n11), but the time of peak firing was constant and coincident [n03, 905 ± 15 (SD) msec; n10, 921 ± 13 msec; n11, 897 ± 21 msec[. *C*, Correlation strengths between the firing rates of cells n03, n10, and n11 and muscle activations. Asterisks, Muscles in which cross-correlations were significant (from left to right: lateral triceps, biceps, pectoralis, medial triceps, deltoid, trapezius, FCU, ECU, ECR, brachialis). *D*, Each M1 cell was significantly correlated with the same IC, which was activated at reach onset. Weights for this IC in the initial and final training segments are shown in the top and bottom bar plots, respectively. *E*, The weights for this IC showed significant changes with training. Weight changes across the first day (relative to the initial training segment) are shown for three muscles [dark gray, brachialis (Bi); light gray, trapezius (Trap); black, deltoid (Delt)]. Weight changes were associated with changes in the ratio of M1 activities that were correlated with this IC.

activity within this group of coactive cells changes how the synergy activation pattern was distributed to muscles.

**Adaptation of muscle synergy activations**

Adapting the balance of muscle activations within a synergy was one mechanism associated with improvement. A second mechanism that was observed in 6 of 11 animals was adaptation of the amplitude of synergy activation alone.

A common finding, which elucidates this mechanism (in three of six animals: rats I, N, and O), was reduced activation of a coherent burst of activity that was distributed to antagonistic muscles around both the shoulder and elbow joints. Figure 10*A* shows the activation pattern of six ICs, which accounted for 79% of the EMG variance in rat N. The third IC to be activated (from the top) was distributed to antagonist muscles at the elbow (triceps muscles and biceps brachii) and at the shoulder (deltoid, teres major, and trapezius). The activation of IC3 was dramatically reduced in the last block compared with the first block of trials (40% reduction in mean integrated area; significant difference in means at $p < 0.001$); in Figure 10*A*, first column, third row, the solid black line represents the mean activation of IC3 in the first block of reach trials, and the dashed line represents the mean activation of IC3 in the last block. Importantly, similarity values between the initial IC3 weights and IC3 weights later in the day were not significantly different than values between most similar locomotor ICs. This indicates that IC3 weights were relatively stable over the training session, whereas only the amplitude of this distributed signal was modified. A similar IC that was widely distributed to antagonist muscles at the shoulder, elbow, and sometimes wrist was activated in the other two animals (rats I and O). In each animal, this "cocontraction" IC was activated most strongly during the limb transport phase before pellet contact and was significantly reduced in magnitude (integrated area) during block 3 compared with block 1. The reduction was not apparent to all ICs constituting the motor pattern and was therefore specific; e.g., IC2, which initiated the reach in rat N, was increased in amplitude in block 3 compared with block 1 (Fig. 10*A*, first column, second row).

The reduced amplitude of IC3 activation in rat N (in combination with increased IC2 amplitude) was correlated with two functional changes: more direct hand paths to the pellet and reduced delay between reach onset and pellet contact. The reduced delay between IC2 activation (reach onset) and pellet contact can be appreciated from Figure 10*A*, in which the trials are aligned at the time of contact [the time between IC2 onset and pellet contact (black vertical line) gradually decreased over time]. Figure 10*B* shows three representative and successive reaching frames for rat N on entry through the aperture (top row, early reach; bottom

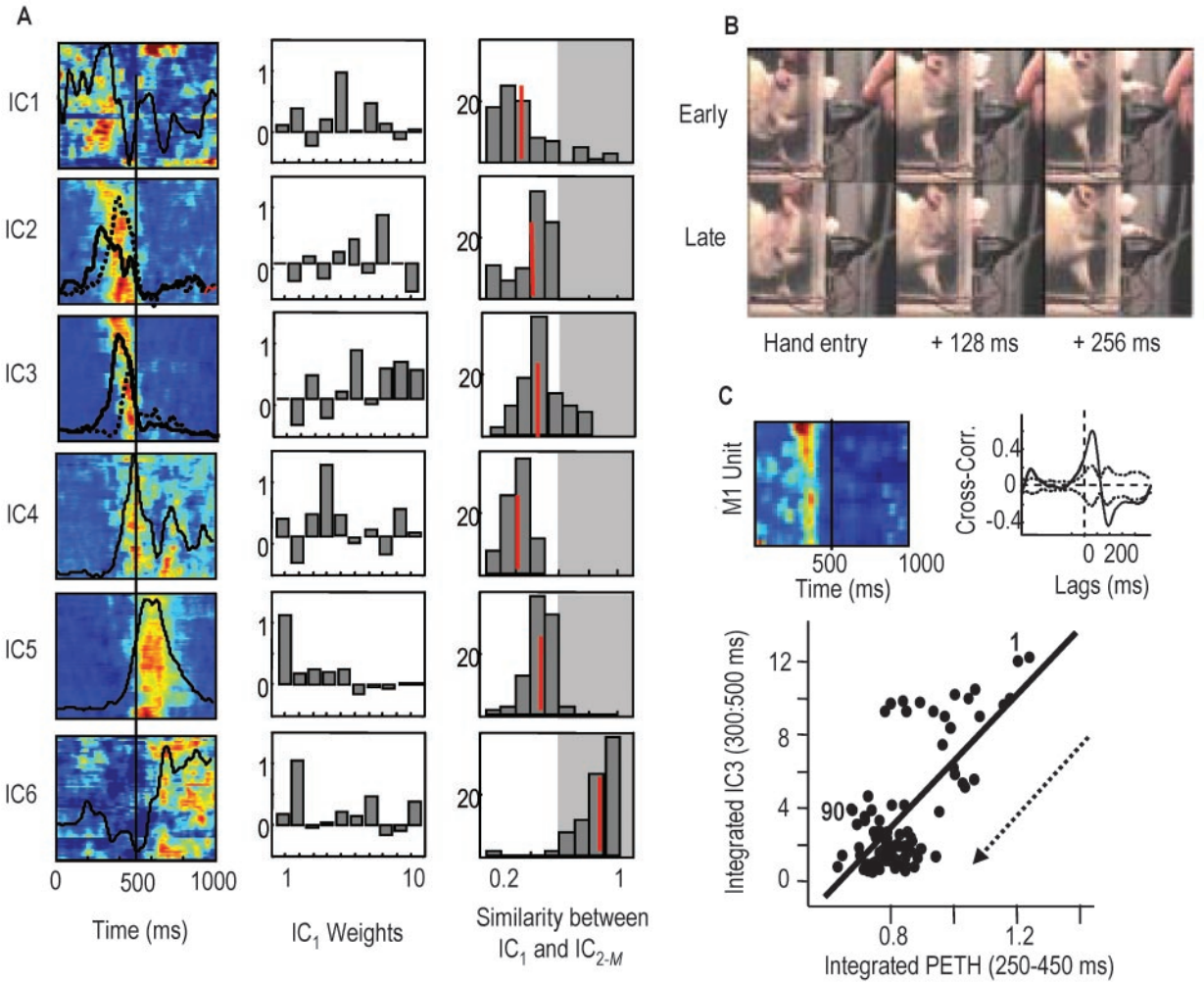


**Figure 10.** Adaptation of the amplitude of synergy activation. *A*, (same as Fig. 7), Contour plots showing activation pattern of six ICs for rat N. Each row is one attempt (90 attempts); red, highest activity. Mean activations are superimposed (black lines, for IC2, IC3; solid lines, mean of block 1; dotted lines, mean of block 3). Bar plots in middle column show IC weights for the first 10 trials (muscles from left to right: FCU, brachialis, medial triceps, lateral triceps, ECR, deltoid, ECU, biceps, trapezius, teres major). ICs were activated sequentially (top to bottom: IC1, prereach posture; IC2, reach initiation; IC3, cocontraction of shoulder and elbow flexors, extensors; IC4, limb extension, hand positioning; IC5, grasping; IC6, retraction). Activation of IC2 was increased, and activation of IC3 was reduced with training. Bar plots in the right last column show the distribution of Euclidean distances between $IC_1$ weights and $IC_{2 \rightarrow M}$ weights, where 1 refers to trials 1–10, 2, trials 2–11, and M, last 10-trial segment. Red lines, Mean distance. IC2 and IC3 weights were not significantly changed during training (see Results, Adaptation of muscle synergy activations). *B*, Representative kinematics for early and late reaches; frames are synchronized to aperture entry. Hand path length was reduced with training. C, Top left, Contour plot of the PETHs of an M1 cell significantly correlated with IC3 activation (cross-correlation shown in the top right graph). Each row represents data from one attempt; red, highest firing rates. Bottom graph, Integrated PETH area (between 250 and 450 msec) versus integrated IC3 area (between 300 and 500 msec). 1, 90, Trial numbers; arrow, direction of IC3 PETH reduction through time. The linear regression was significant at $p < 0.01$ ($R^2 = 0.49$).

row, late reach). In the early reach, the hand followed a more curved path to the pellet because the limb was raised higher relative to the tray and was held above the tray for a longer period (i.e., presumably because of increased muscle cocontraction). The normalized path lengths (of the hand to the pellet) were computed for the first and last blocks for the three animals showing reduction of this cocontraction IC. We found a small but significant reduction in path length over time [at $p < 0.05$; first block, 1.35 ± 0.11 (SD); last 20, 1.20 ± 0.10) and a significantly reduced delay between initial IC activation and pellet contact (first block, 330 ± 17 msec; last block, 279 ± 17 msec). These changes were associated with improved success rates.

Ten of 37 M1 cells that were significantly correlated with muscle activations were positively correlated with stable ICs (correlated with 1.13 ± 0.35 ICs; i.e., seven of eight were correlated with just one IC, and one cell was correlated with two ICs). Stable ICs were those in which the mean Euclidean distance between weights over the day was not significantly different from the mean distance between the weights of most similar locomotor ICs; 31 of 66 or 47% of ICs (six ICs per animal, which described 65–75% of EMG variance, 11 animals) were considered stable. Mean peak correlations for these 10 cells with IC activation patterns were 0.21 ± 0.7 (SD). Of the 10 cells, 8 had significantly increased or decreased peak rates in block 3 compared with block 1 ( $p < 0.01$; 6 of 8 were decreased by 14 ± 6 Hz; 2 of 8 were increased by 11 ± 3 Hz). These rate changes were accompanied by corresponding changes in the activation magnitude of ICs to which they were correlated. Figure 10*C* shows data for an M1 cell (in rat N) that had firing rates correlated with IC3 activation. The left panel shows firing rates for this cell, in which each row is data for one trial (red is highest activity), and the right graph shows the cross-correlation between the firing rate of this cell and IC3 activation. Both IC3 magnitude (Fig. 10*A*) and the firing rate of the cell were reduced with training. Figure 10*C*, bottom graph, shows

a scatterplot of the integrated area of the PETH (250–450 msec) versus the integrated area of IC3 activation (300–500 msec). The linear regression was significant ( $p < 0.01$; $R^2 = 0.50$). All eight cells that were correlated with stable ICs showed significant linear relationships between integrated PETH area ($t - t + 200$ msec; $t$ is time) and integrated IC area ($t + 50 - t + 250$); all were significant at $p < 0.05$, and 3 were significant at $p < 0.01$. The mean $R^2$ statistic was $0.41 \pm 0.07$ (SD). These findings suggest that M1 cells and muscle synergies could be regulated as a coherent unit, and this unit was in certain cases related to a widespread cocontraction signal.

## Discussion

### Muscle synergies and motor programs

Muscle synergies were defined in the present study as ICs. ICs were extracted from EMG patterns with the statistical algorithm called ICA (Makeig et al., 1997). In its application, we assumed that each EMG channel received activation from several source signals originating in the CNS, and each source distributed its signal to multiple muscles. ICA was used to estimate these source signals and their distribution patterns. That ICs exhibited all-or-nothing activation patterns (e.g., switching), that ICs could be individually regulated (e.g., activation amplitude) without affecting other ICs, that M1 firing patterns were correlated with IC activations, and that the sequences and distribution patterns (weights) of ICs were consistent among animals provide evidence that ICs, or muscle synergies, may indeed be represented in the CNS (see below).

We distinguished between muscle synergies and motor programs by defining motor programs as sequences of synergy activation. We focused on sequences (of three or four synergies) that occurred between reach onset and pellet contact. Because corrective submovements appeared only after pellet contact (Whishaw et al., 1998), animals probably relied heavily on accurate feedforward control of this movement portion. Such feedforward patterns have been termed motor programs (Morris et al., 1994) and are thought to represent the output of a pattern generator or internal controller (Shadmehr and Mussa-Ivaldi, 1994; Wolpert and Kawato, 1998; Wolpert et al., 2001). That animals switched between motor programs provides evidence that discrete CNS controllers may have generated these patterns. Interestingly, animals improved early performance by increasing the probability of activating the more successful controller.

### Motor pattern adaptation

Early improvements were also related to the appropriate adaptation of selected motor programs. Adaptation occurred at the level of both individual muscles and muscle synergies. Animals appeared to reconfigure preexisting muscle synergies with training (Porter and Lemon, 1993; Nudo et al., 1996; Wolpert et al., 2001). We quantified this by determining how the distribution of coherent muscle activities (IC weights) changed during training relative to the weights of locomotor ICs, which are likely to be stable. Animals modified the weights of one or two synergies during training, and most animals modified one synergy in particular, which was distributed to extrinsic hand muscles and activated just before pellet contact. These weight changes were associated with changes in hand and finger kinematics before pellet contact and with improved grasping. The adaptation of IC weights provides evidence that animals regulated motor patterns at the level of individual muscles.

Animals also regulated motor patterns at the level of individual synergies, i.e., modified the amplitude of synergy activations without changing the balance of muscle activities within the synergy. We referred to these synergies as being stable. Regulation of the amplitude and onset times of a small number of stable synergies potentially accelerates learning by reducing the degrees of freedom of the activation parameter space (Winters, 2000). In support of this, we found that animals commonly adjusted the amplitude of several stable synergies in parallel (e.g., Fig. 10, in which IC2 was increased in amplitude and IC3 was simultaneously decreased during training). Animals reduced the amplitude of one synergy in particular that was distributed to antagonistic muscles around the shoulder, elbow, and wrist. This adjustment was associated with straighter hand paths, reduced movement times, and improved targeting. Humans similarly regulate the amplitude of a widespread cocontraction signal during motor learning and thus rely less on viscoelastic properties of the limb (Thoroughman and Shadmehr, 1999; Osu et al., 2002).

Most animals (8 of 11) activated the same basic motor pattern from the onset of training, i.e., did not exhibit switching. This suggests that a motor pattern and synergies were learned already, were innately specified (Whishaw et al., 1998; Tresch and Bizzi, 1999), were quickly adapted from other behaviors (e.g., locomotion; Georgopoulos and Grillner, 1989), or were careless solutions wherein reasonable success rates obtained with initial, approximate solutions did not induce alternative search paths (Scheidt et al., 2001). Nonetheless, that success rates increased by 20% on the first day and 50% over the following 10 d supports the idea that module tuning is an important component to skill learning (Mussa-Ivaldi and Bizzi, 2000).

### Motor cortical basis for early skill learning

Although M1 may contribute to learning itself (Pascual-Leone et al., 1994; Sanes and Donoghue, 2000; Li et al., 2001; Muellbacher et al., 2002), our results address the role of M1 in expressing learning-related mechanisms. These mechanisms were related to action selection and motor adaptation. We found that prereach M1 activity predicted significantly above chance the switching between motor patterns. Prereach muscle activity was not as effective. Thus, prereach M1 activity appeared to reflect both motor-related output and sensory input (Asanuma, 1981; Evarts, 1981; Singh and Scott, 2003), and this information may contribute to state estimation (Naito et al., 2002) and action selection (Kettner et al., 1996; Carpenter et al., 1999; Laubach et al., 2000).

M1 cells (37%) had firing rates during the task that were significantly correlated with the activation of multiple muscles (McKiernan et al., 2000; Holdefer and Miller, 2002) and with primarily one IC. The mean latency for M1–IC and M1–muscle correlations was ~ 60 msec, which is in the range observed for M1–muscle correlations in monkeys (50–75 msec; Morrow and Miller, 2003). That latencies were not shortened in rats (e.g., because of shorter conduction lines) suggests that the average (effective) synapse number from M1 to muscles might be increased or that conduction velocities might be reduced. At these latencies, the mean firing rates of individual cells appeared very similar to the activation patterns of ICs (see Fig. 8). However, cells were in most cases significantly correlated with only a subset of muscles that constituted the IC (on average, 3.5 of 5 muscles). Thus, a population of coactive M1 cells rather than individual cells specifies the IC activation pattern (i.e., both the weights and activation waveform; the activation waveform itself may be specified by individual cells).

M1 cell pairs were recorded that had a high probability of coincident spiking during the task and that were correlated with the same IC. Coincident spiking is common among M1 cells (Fetz

et al., 1991; Hatsopoulos et al., 2001; Schieber, 2002), especially those with overlapping muscle projections (Jackson et al., 2003). The peak firing rates of these coactive cells were regulated either proportionately or disproportionately during training. We suggested that disproportionate or opposite changes in the firing rates of coactive cells underlie changes in how the IC activation pattern was distributed to muscles (see Fig. 9; adaptation of IC weights). However, establishing a direct correspondence between IC weight changes and firing rate changes is likely to be difficult because tens of cells appear to control any one muscle activation pattern (Morrow and Miller, 2003), and cells may be correlated with overlapping but slightly different sets of muscles (McKiernan et al., 2000). In contrast to weight changes, we suggested that changes in the amplitude of synergy activation were likely to be attributable to in-parallel and proportionate changes in the firing rates of coactive cells (Fig. 10). Because only a small population of coactive cells was recorded, which were correlated with the same IC (three cells at the most), this was again difficult to prove definitively. Despite this, our data support the existence of functional M1 assemblies (coactive cells) that specify synergy activations and that form tunable modules during learning.

Many cells (63%) were not correlated with forelimb muscle activations on day 1. Seventy-six percent of these cells (48 of 63) had significantly increased or decreased firing rates in block 3 compared with block 1 and thus were adapted with training. These cells might instead specify kinematics (Georgopoulos et al., 1986; Kakei et al., 1999; Reina et al., 2001), dynamics (Li et al., 2001; Gribble and Scott, 2002), posture (Sergio and Kalaska, 2003), or pellet location, alone or in combination (Fu et al., 1995). Alternatively, some of these cells might encode only the onset or amplitude of synergy activations rather than the time course, which is encoded elsewhere (e.g., spinal cord; Tresch and Bizzi, 1999). Furthermore, extended training might enhance the apparent connectivity between M1 cells and muscles through changes in M1 reliability, synchrony, or both (Schieber, 2002). Finally, it is unclear whether cells were pyramidal tract cells (PTNs), corticomotoneuronal cells, or M1 interneurons, which will affect parameter encoding (Beloozerova et al., 2003). However, we expect that many cells were PTNs (electrolytic lesions were in layer V in all animals).

In summary, the present study showed that early skill learning was expressed through motor program selection and tuning. Selection was predicted in part by prereach M1 activity. Reach-related M1 activity was correlated with the activation of specific muscle synergies. This M1 activity was adapted with training, and these changes were associated with changes in either the amplitude of activation or composition of the correlated synergy. Both forms of motor pattern tuning were associated with performance improvements.

## References


Asanuma H (1981) Functional role of sensory inputs to the motor cortex. Prog Neurobiol 16:241–262.

Beloozerova IN, Sirota MG, Swadlow HA (2003) Activity of different classes of neurons of the motor cortex during locomotion. J Neurosci 23:087–97.

Bernstein NA (1967) The coordination and regulation of movements. Oxford: Pergamon.

Bury SD, Jones TA (2002) Unilateral sensorimotor cortex lesions in adult rats facilitate motor skill learning with the "unaffected" forelimb and training-induced dendritic structural plasticity in the motor cortex. J Neurosci 22:8597–8606.

Carpenter AF, Georgopoulos AP, Pellizer G (1999) Motor cortical encoding of serial order in a context-recall task. Science 283:1752–1757.

D'Avella A, Saltiel P, Bizzi E (2003) Combinations of muscle synergies in the construction of a natural motor behavior. Nat Neurosci 6:300–308.

Earhart GM, Stein PS (2000) Scratch-swim hybrids in the spinal turtle: blending of rostral scratch and forward swim. J Neurophysiol 83:156–165.

Evarts EV (1981) Role of motor cortex in voluntary movements in primates. In: Handbook of physiology (Brooks VB, ed), pp 1083–1120. Baltimore: Williams & Wilkins.

Fetz EE, Toyama K, Smith W (1991) Synaptic interactions between cortical neurons. In: Cerebral cortex (Peters A, Jones EG, eds), pp 1–80. New York: Plenum.

Fu QG, Flament D, Coltz JD, Ebner TJ (1995) Temporal encoding of movement kinematics in the discharge of primate primary motor and premotor neurons. J Neurophysiol 73:836–854.

Georgopoulos AP, Grillner S (1989) Visuomotor coordination in reaching and locomotion. Science 245:1209–1210.

Georgopoulos AP, Schwartz AB, Kettner RE (1986) Neuronal population coding of movement direction. Science 233:1416–1419.

Graziano MS, Taylor CS, Moore T, Cooke DF (2002) The cortical control of movement revisited. Neuron 36:349–362.

Gribble PL, Scott SH (2002) Overlap of internal models in motor cortex for mechanical loads during reaching. Nature 417:938–941.

Grillner S (1981) Control of locomotion in bipeds, tetrapods and fish. In: Handbook of physiology, Sect I, The nervous system (Brooks VB, ed), pp 1179–1236. Bethesda, MD: American Physiological Society.

Hatsopoulos NG, Harrison MT, Donoghue JP (2001) Representations based on neuronal interactions in motor cortex. Prog Brain Res 130:233–244.

Holdefer RN, Miller LE (2002) Primary motor cortical neurons encode functional muscle synergies. Exp Brain Res 146:233–243.

Hyland B, Jordan VM (1997) Muscle activity during forelimb reaching movements in rats. Behav Brain Res 85:175–186.

Jackson A, Gee VJ, Baker SN, Lemon RN (2003) Synchrony between neurons with similar muscle fields in monkey motor cortex. Neuron 38:115–125.

Kakei S, Hoffman DS, Strick PL (1999) Muscle and movement representations in the primary motor cortex. Science 285:2136–2139.

Kargo WJ, Giszter SF (2000a) Rapid correction of aimed movements by summation of force-field primitives. J Neurosci 20:409–426.

Kargo WJ, Giszter SF (2000b) Afferent roles in hindlimb wipe-reflex trajectories: free-limb kinematics and motor patterns. J Neurophysiol 83:1480–1501.

Karni A, Meyer G, Rey-Hipolito C, Jezzard P, Adams MM, Turner R, Ungerleider LG (1998) The acquisition of skilled motor performance: fast and slow experience-driven changes in primary motor cortex. Proc Natl Acad Sci USA 95:861–868.

Kettner RE, Marcario JK, Port NL (1996) Control of remembered reaching sequences in monkey. II. Storage and preparation before movement in motor and premotor cortex. Exp Brain Res 112:347–358.

Kleim JA, Barbay S, Nudo RJ (1998) Functional reorganization of the rat motor cortex following motor skill learning. J Neurophysiol 80:3321–3325.

Kleim JA, Barbay S, Cooper NR, Hogg TM, Reidel CN, Remple MS, Nudo RJ (2002) Motor learning-dependent synaptogenesis is localized to functionally reorganized motor cortex. Neurobiol Learn Mem 77:63–77.

Laubach M, Wessberg J, Nicolelis MAL (2000) Cortical ensemble activity increasingly predicts behavior outcomes during learning of a motor task. Nature 405:567–571.

Li CS, Padoa-Schioppa C, Bizzi E (2001) Neuronal correlates of motor performance and motor learning in the primary motor cortex of monkeys adapting to an external force field. Neuron 30:593–607.

Makeig S, Jung TP, Bell AJ, Ghahremani D, Sejnowski TJ (1997) Blind separation of auditory event-related brain responses into independent components. Proc Natl Acad Sci USA 94:10979–10984.

McKiernan BJ, Marcario JK, Karrer JH, Cheney PD (2000) Correlations between cortico-motoneuronal (CM) cell postspike effects and cell-target muscle covariation. J Neurophysiol 83:99–115.

Miller LE, van Kan PL, Sinkjaer T, Andersen T, Harris GD, Houk JC (1993) Correlation of primate red nucleus discharge with muscle activity during free-form arm movements. J Physiol (Lond) 469:213–243.

Morris ME, Summers JJ, Matyas TA, Iansek R (1994) Current status of the motor program. Phys Ther 74:738–748.

Morrow MM, Miller LE (2003) Prediction of muscle activity by populations of sequentially recorded primary motor cortex neurons. J Neurophysiol 89:2279–2288.

Muellbacher W, Ziemann U, Wissel J, Dang N, Kofler M, Facchini S, Boroojerdi B, Poewe W, Hallett M (2002) Early consolidation in human primary motor cortex. Nature 415:640–644.

Mussa-Ivaldi FA, Bizzi E (2000) Motor learning through the combination of primitives. Philos Trans R Soc Lond B Biol Sci 355:1755–1769.

Naito E, Roland PE, Ehrsson HH (2002) I feel my hand moving: a new role of the primary motor cortex in somatic perception of limb movement. Neuron 36:979–988.

Nudo RJ, Milliken GW, Jenkins WM, Merzenich MM (1996) Use-dependent alterations of movement representations in primary motor cortex of adult squirrel monkeys. J Neurosci 16:785–807.

Osu R, Franklin DW, Kato H, Gomi H, Domen K, Yoshioka T, Kawato M (2002) Short- and long-term changes in joint co-contraction associated with motor learning as revealed from surface EMG. J Neurophysiol 88:991–1004.

Pascual-Leone A, Grafman J, Hallett M (1994) Modulation of cortical motor output maps during development of implicit and explicit knowledge. Science 263:1287–1289.

Poe GR, Nitz DA, McNaughton BL, Barnes CA (2000) Experience-dependent phase-reversal of hippocampal neuron firing during REM sleep. Brain Res 855:176–180.

Porter R, Lemon R (1993) Corticospinal function and voluntary movement. Oxford: Clarendon.

Raasch CC, Zajac FE (1999) Locomotor strategy for pedaling: muscle groups and biomechanical functions. J Neurophysiol 82:515–525.

Reina GA, Moran DW, Schwartz AB (2001) On the relationship between joint angular velocity and motor cortical discharge during reaching. J Neurophysiol 85:2576–2589.

Rioult-Pedotti MS, Friedman D, Hess G, Donoghue JP (1998) Strengthening of horizontal cortical connections following skill learning. Nat Neurosci 1:230–234.

Rioult-Pedotti MS, Friedman D, Donoghue JP (2000) Learning-induced LTP in neocortex. Science 290:533–536.

Sanes JN, Donoghue JP (2000) Plasticity and primary motor cortex. Annu Rev Neurosci 23:393–415.

Scheidt RA, Dingwell JB, Mussa-Ivaldi FA (2001) Learning to move amid uncertainty. J Neurophysiol 86:971–978.

Schieber MH (2002) Training and synchrony in the motor system. J Neurosci 22:5277–5281.

Sergio LE, Kalaska JF (2003) Systematic changes in motor cortex cell activity with arm posture during directional isometric force generation. J Neurophysiol 89:212–228.

Shadmehr R, Mussa-Ivaldi FA (1994) Adaptive representation of dynamics during learning of a motor task. J Neurosci 14:3208–3224.

Singh K, Scott SH (2003) A motor learning strategy reflects neural circuitry for limb control. Nat Neurosci 6:399–403.

Stone JV (2002) Independent components analysis: an introduction. Trends Cogn Sci 6:59–64.

Thoroughman KA, Shadmehr R (1999) Electromyographic correlates of learning an internal model of reaching movements. J Neurosci 19:8573–8588.

Tresch MC, Bizzi E (1999) Responses to spinal microstimulation in the chronically spinalized rat and their relationship to spinal systems activated by low threshold cutaneous stimulation. Exp Brain Res 129:401–416.

Tresch MC, Saltiel P, Bizzi E (1999) The construction of movement by the spinal cord. Nat Neurosci 2:162–167.

Whishaw IQ, Gorny B (1996) Does the red nucleus provide the tonic support against which fractionated movements occur? A study on forepaw movements used in skilled reaching by the rat. Behav Brain Res 74:79–90.

Whishaw IQ, Gorny B, Sarna J (1998) Paw and limb use in skilled and spontaneous reaching after pyramidal tract, red nucleus and combined lesions in the rat: behavioral and anatomical dissociations. Behav Brain Res 93:167–183.

Winters JM (2000) Study of movement selection and synergies via a neuro-optimization framework. In: Biomechanics and neural control of posture and movement (Winters JM, Crago PE, eds), pp 458–473. New York: Springer.

Wise SP, Moody SL, Blomstrom KJ, Mitz AR (1998) Changes in motor cortical activity during visuomotor adaptation. Exp Br Res 121:285–299.

Wolpert DM, Kawato M (1998) Multiple paired forward and inverse models for motor control. Neural Netw 11:1317–1329.

Wolpert DM, Ghahramani Z, Flanagan JR (2001) Perspectives and problems in motor learning. Trends Cogn Sci 5:487–494.